Welding in the World (2018) 62:713–719
https://doi.org/10.1007/s40194-018-0581-y

RESEARCH PAPER

Precipitates in microalloyed ultra-high strength weld metal studied by atom probe tomography

Phillip Haslberger[1] · Sylvia Holly[2] · Wolfgang Ernst[3] · Ronald Schnitzer[1]

Received: 15 September 2017 / Accepted: 10 March 2018 / Published online: 3 April 2018

Abstract
Gas metal arc welding with metal-cored filler wires is frequently used to weld high strength steel constructions for lightweight and transportation applications. In the current study, microalloying is considered as strengthening concept for reaching the required mechanical properties by precipitation hardening. For this purpose, the typical microalloying elements Ti, Nb, V, and Al were added to the filler metal in a comparatively high amount (up to 0.5 m.%). All-weld metal samples with a yield strength of 1000 MPa and more were produced by gas metal arc welding. Laser-pulsed atom probe tomography was used to evaluate the potential of these elements to form clusters or precipitates and strengthen the weld metal. While Al and Nb did not form clusters, a strong tendency for clustering was found for V- and Ti-alloyed samples. The cluster size evolution and changes in chemical composition depending on the microalloying contents are discussed. Furthermore, the challenges arising from local alloying element enrichments and local differences in thermal history in the all-weld metal are addressed regarding sample preparation and data evaluation.

Keywords Filler materials · Weld metal · Microalloying · Microstructure · Atom probe tomography · Sampling

1 Introduction

Welding of steels with matching filler materials promises a well-balanced property profile over the entire construction. High strength steels are currently used for cranes, cantilevers, or lightweight applications. Sheets with a yield strength up to 1300 MPa are readily available, which results in the need for matching welding consumables. In the field of welding, the trade-off between strength and toughness of the material is ubiquitous because of the limited applicability of thermomechanical processing after welding. Therefore, an elaborate alloy design is crucial for good service properties.

Recommended for publication by Commission II - Arc Welding and Filler Metals

✉ Phillip Haslberger
phillip.haslberger@unileoben.ac.at

[1] Department of Physical Metallurgy and Materials Testing, Montanuniversität Leoben, Franz-Josef-Strasse 18, 8700 Leoben, Austria

[2] voestalpine Böhler Welding Austria GmbH, Kapfenberg, Austria

[3] voestalpine Stahl GmbH, Linz, Austria

With high strength steel welds, the best results were achieved by using the well-known microalloying elements Al and Ti for modifications of the inclusions, which resulted in a high amount of acicular ferrite [1, 2]. Acicular ferrite was established as a favored microstructure in steel welds [3–5]. However, the strength of acicular ferrite is limited. In order to create the next generation of steel welds, stronger microstructures like martensite mixed with bainitic constituents had to be considered. This yielded welds with a yield strength of approx. 1000 MPa [6, 7].

Currently, experiments are running with the goal of developing a filler material with a yield strength of 1100 MPa. Several alloying systems were used in previous studies, leading to promising results regarding both strength and toughness [8, 9]. In these studies, high-resolution imaging methods were applied to analyze the microstructure of the welds [9]. It was shown that microalloying can serve as an alternative concept for welds regarding strengthening [8]. A combination of Ti, Nb, and Al increased the strength of the welds effectively, as was predicted by thermodynamic and kinetic simulations. However, the type and nature of the presumably existing precipitates were not described in detail.

The microalloying elements Ti, Nb, Al, and V are well known for their beneficial effects in several types of materials

[10–12]. Because of their low solubility in ferrite, microalloy carbides and nitrides are very stable. They can form in several temperature and phase regions and are usually of MX-type. Regarding strength, precipitates formed in a supersaturated ferrite during reheating of the material are most effective [12].

One way to characterize the particles resulting from microalloying is using atom probe tomography [13]. The combination of nearly atomic resolution and information on the chemical identity of the measured atoms can deliver deep insights in the precipitation behavior of a material [14]. This has been used to identify precipitates in steels microalloyed with the classical microalloying elements, like Ti, Nb, V, or Al [15–19], but also to identify clusters resulting from Cu additions [20, 21] or to investigate numerous other alloy systems. Recently, a method was established to directly observe hydrogen trapping in a material [22], which could be of great value for the welding community.

Nevertheless, in the research field of welding, only few investigations involving atom probe tomography can be found. A good overview of the early use of atom probe on weld metals was given by Vitek and Babu [23]. In the last few years, atom probe tomography was mainly used to characterize the precipitation behavior of Cu-bearing pressure vessel steel welds [21, 24–27] or to study welds of more exotic materials like Y-rich Ti-5111 [28], friction stir welds of nanostructured ferritic alloys [29], or dissimilar metal welds [30].

The current paper intends to point out the potential of using atom probe tomography for weld metal. A procedure for sample preparation and data evaluation for the special case of multi-layer weld metal is suggested. The method is used to investigate several differently microalloyed samples regarding their cluster and precipitate populations. By comparing these microstructural features with the resulting strength of the weld metal, this should clarify which microalloying elements have the highest strengthening potential for steel welds.

2 Materials and methods

The investigated all-weld metal samples were produced by gas metal arc welding according to DIN EN ISO 15792-1. A macro-etched cross-section of such an all-weld metal is shown in Fig. 1. Two groups of alloys were designed to investigate the influence of different microalloying elements on the precipitation characteristics.

In the first group, several microalloying elements were added to the reference filler material, namely Ti, Nb, V, Al, and N. The chemical composition of the alloys was measured by optical emission spectroscopy and is stated in Table 1. The

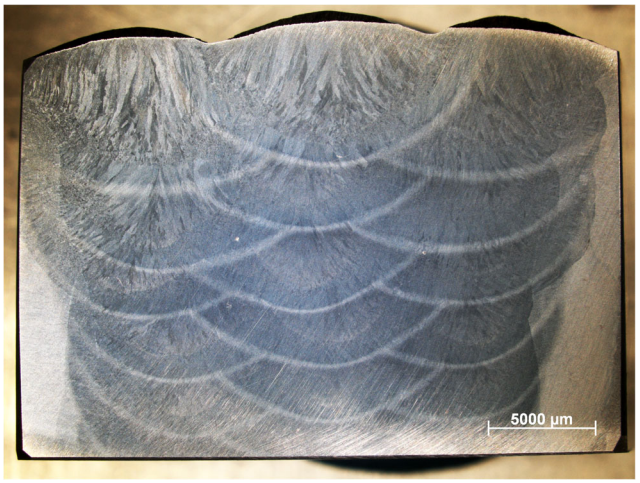

Fig. 1 Cross-section of an all-weld metal sample, macro-etched with nital

O content was 400–500 ppm in all alloys. With this first alloy group, it was intended to test the general effect of microalloying on the weld metal properties.

In the second group, the microalloying elements were separated to clarify, which elements were driving the precipitation process. Therefore, specimens were fabricated containing V and Al separately (Table 2). Please note that an inherent content of ca. 50 ppm N and 100 ppm Ti is also present in alloys without an intended N or Ti addition.

The tensile strength of the samples was determined by tensile tests at room temperature according to EN ISO 6892-1 after a soaking treatment at 150 °C for 16 h to remove residual H.

For the characterization of the precipitates, atom probe tomography was used. The atom probe measurements were performed in a Cameca LEAP 3000 X HR in laser mode with the following parameters: temperature 60 K, pulse repetition rate 250 kHz, laser energy 0.3 nJ, target evaporation rate 1%. The specimens were prepared by cutting rods in welding direction with a cross-section of 0.3×0.3 mm^2, followed by the well-known electrolytic two-step process [31] to generate sufficiently sharp tips. The specimen radius should be in the range of 10 to 50 nm. For an elaborate explanation of this two-step process and guidelines for the preparation of different materials, please refer to [32].

Generally, all tips were prepared from random locations within the all-weld metal. Therefore, the thermal history of the tips cannot be specifically stated. Due to the multi-layer welding, a bead is reheated shortly by the following welding beads. Per alloy, 10 measurements at random locations were performed to gain statistically relevant results regarding the average precipitate population in the alloy.

In order to clarify, whether some of the precipitates formed during the initial cooling of the bead or all of them formed during reheating, additional samples of the last deposited bead (top middle bead in Fig. 1) were taken from alloy 0.5V,

Table 1 Chemical composition of the alloys in group 1 and the reference alloy

Group 1—Ti-Nb-Al-V								
	C (m.%)	Si (m.%)	Mn (m.%)	Ti (m.%)	Nb (m.%)	Al (m.%)	V (m.%)	N (m.%)
Reference	0.11	0.82	2.63	0.01	–	–	–	0.008
Ti-Nb-Al	0.10	0.91	2.67	0.04	0.08	0.02	–	0.02
Ti-Nb-Al-0.2V	0.10	0.92	2.65	0.05	0.08	0.03	0.22	0.02
Ti-Nb-Al-0.5V	0.10	0.89	2.63	0.04	0.08	0.02	0.50	0.02

Table 2 Chemical composition of the alloys in group 2

Group 2—influence of single elements								
	C (m.%)	Si (m.%)	Mn (m.%)	Ti (m.%)	Nb (m.%)	Al (m.%)	V (m.%)	N (m.%)
Al	0.08	0.76	2.40	0.01	–	0.02	–	0.005
0.3V	0.09	0.55	1.24	0.01	–	–	0.31	0.004
0.5V	0.08	0.57	1.27	0.01	–	–	0.52	0.005

followed by the same measuring and evaluation protocol as for all other samples.

After the measurement, the reconstructed tips were scanned for clusters or precipitates using isosurfaces and nearest neighbor distributions [33, 34]. Both of these methods are used for visualizing local enrichments of atoms with the same chemical identity. Enriched areas were exported in separate files before analyzing the chemical composition of these exported clusters or precipitates.

3 Results

3.1 Alloy group 1

The tensile tests showed that the combined addition of Ti, Nb, and Al resulted in a significant strength increase compared to the reference sample (Table 3), which was already shown in [8]. By adding V in a comparatively high amount (0.2 m.%), the strength could be improved further. Increasing the amount of V to 0.5 m.% again brought additional strength.

The microstructural investigations with the atom probe revealed precipitates in the order of 1 to 10 nm. An exemplary image of a reconstruction of a tip from the alloy Ti-Nb-Al-0.5V is shown in Fig. 2. The pink dots represent Fe atoms in the ferritic matrix. In blue, isoconcentration surfaces are depicted, visualizing local enrichments of Ti, V, C, and N with an added content of >20 at.%. Therefore, in this case, precipitates containing Ti, V, C, and N were found. Size and chemistry varied within each alloy and within each measured tip and also depended on the alloy system itself. These variations are addressed in Section 4.

The evolution of the average precipitate chemistry and size depending on the alloy composition is shown in Table 4. In the sample Ti-Nb-Al, the precipitates contain mainly Ti and C.

Table 3 Tensile properties of the samples from group 1

Mechanical properties: group 1—Ti-Nb-Al-V		
	R_m (MPa)	$R_{p0.2}$ (MPa)
Reference	1128	1006
Ti-Nb-Al	1204	1082
Ti-Nb-Al-0.2V	1258	1139
Ti-Nb-Al-0.5V	1272	1164

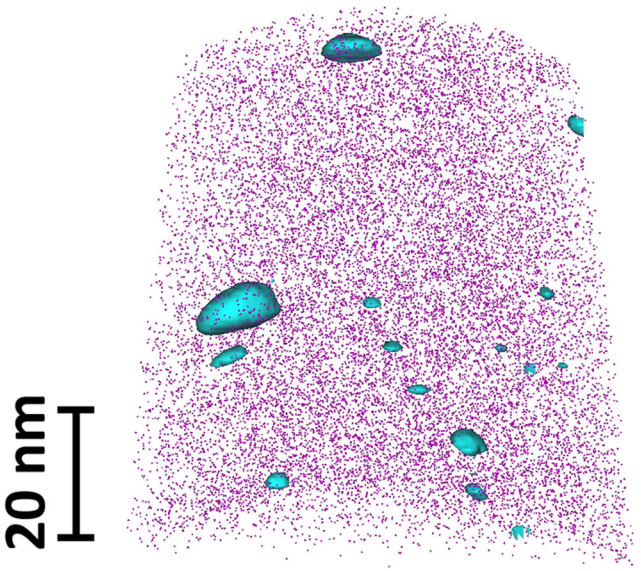

Fig. 2 Exemplary image of a reconstruction of an atom probe measurement of a microalloyed sample. Pink dots represent iron atoms. The blue isoconcentration surfaces show enrichments in Ti, V, C, and N and represent the precipitates

There is still much Fe dissolved in the precipitates, whereas only little Nb and N were found in the precipitates. Al is completely missing in Table 4 because it was always homogeneously distributed in the atom probe sample (exemplarily shown in Fig. 3). The precipitates had a size from 1 to 5 nm. An addition of V changed the average precipitate chemistry fundamentally. The precipitates contained approximately equal amounts of Ti, V, N, and C. Only little Fe was measured, most of which was close to the shell of the precipitates. An increase from 0.2V to 0.5V resulted in no changes in precipitate chemistry but enhanced the average size of the precipitates from 5 nm to approx. 10 nm.

The remaining V content in the steel matrix was investigated by exporting and analyzing a cylindrical region of interest which did not contain any precipitates (Fig. 4). Although a significant amount of V was incorporated in the precipitates, 80 to 90% of all V atoms were still dissolved in the steel matrix in both alloys.

3.2 Alloy group 2

In Table 5, the tensile properties of the samples from group 2 are compared to the reference sample. The Al sample did not show any improvement in strength. Contrarily, an addition of V led to a strength increase, similarly to the V samples in group 1. Especially, the yield strength was drastically improved. In all cases, the formed precipitates were investigated with the atom probe.

The atom probe measurements of the Al-alloyed sample revealed that Al is again homogeneously distributed and does not show any signs of clustering (Fig. 3).

In the 0.3V sample, early clustering signs were identified. From the nearest neighbor distributions, it can be seen that V starts to cluster first, before attracting C and N to form nanometer-sized precipitates. The average chemical composition of these V(C,N) clusters is shown in Table 6.

The increase from 0.3V to 0.5V led to significant changes in amount, size, and chemistry of the clusters (Table 6). Many more clusters occurred in the 0.5V sample, which were also bigger in size. The amount of N dissolved in the clusters dropped drastically due to the limited amount of N available in the alloy, resulting in V-C precipitates. In both cases, a high amount of Fe was measured in the clusters and precipitates, coming again mainly from the shell regions of the clusters and precipitates.

Also, in this group, the V content in the steel matrix was evaluated. In the 0.3V sample, 80 to 90% of all V atoms remained in the matrix. This value drops to approx. 65% for the 0.5V sample.

Table 4 Evolution of the average chemical composition in at.% and size of the precipitates in the alloys of group 1. The rest to 100 at.% in each average chemical composition accounts for matrix elements, which were neglected for the interpretation of the results

Element	Ti-Nb-Al	Ti-Nb-Al-0.2V	Ti-Nb-Al-0.5V
Ti	22 ± 10	15 ± 4	17 ± 4
Nb	6 ± 2	8 ± 4	7 ± 1
V	–	18 ± 2	19 ± 6
N	7 ± 4	15 ± 4	20 ± 4
C	15 ± 13	19 ± 4	17 ± 4
Fe	40 ± 8	14 ± 3	12 ± 4
Precipitate size	1–5 nm	5 nm	10 nm

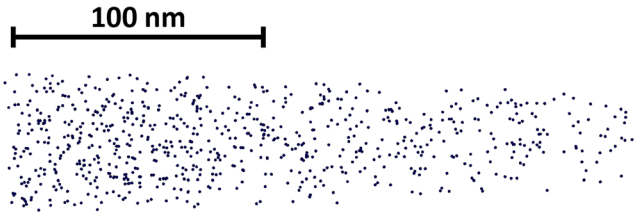

Fig. 3 Example of Al atoms in an Al-alloyed sample. The Al atoms are homogeneously distributed and showed no sign of clustering

4 Discussion

The main objective of this paper was to clarify, if microalloying induces precipitation and therefore strengthening in all-weld metal samples. Furthermore, it was evaluated which microalloying elements were most effective in strengthening. Microalloy carbides and nitrides are known to be very stable and generally have a positive effect on the mechanical properties in a variety of steels [10]. Nevertheless, the amount of precipitates found in the samples and their effect on the mechanical properties in the case of the all-weld metal was unknown so far.

Before the effectiveness of the different microalloying elements is discussed, some methodological issues should be elaborated. The all-weld metal is a multi-layer structure, in which every layer has its own reheated zone. The temperature profile measured with thermocouples in [35]

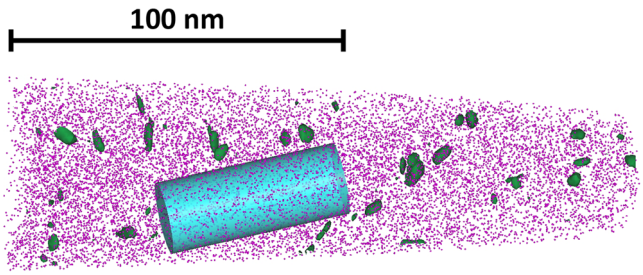

Fig. 4 Reconstruction of an atom probe measurement of a V-alloyed sample. The existence of small V-rich precipitates is evident. The cylindrical region of interest was exported to analyze the remaining V content in the steel matrix

Table 5 Tensile properties of the samples from group 2

Mechanical properties: group 2—single el.		
	R_m (MPa)	$R_{p0.2}$ (MPa)
Reference	1128	1006
Al	1109	998
0.3V	1155	1100
0.5V	1181	1128

Table 6 Evolution of the average chemical composition in at.% and size of the clusters in the alloys of group 2. The rest to 100 at.% in each average chemical composition accounts for matrix elements, which were neglected for the interpretation of the results

Element	0.3V	0.5V
V	34 ± 3	30 ± 2
N	14 ± 2	2 ± 0.4
C	11 ± 3	26 ± 2
Fe	31 ± 6	25 ± 4
Precipitate size	1–3 nm	5 nm

suggests three reheating peaks with temperatures ranging from 300 to 600 °C for a weld bead coming from the subsequently deposited beads. The time of reheating is only a few seconds for each peak.

Firstly, the moment of formation of the precipitates had to be determined. Thermodynamic and kinetic simulations predicted that the majority of precipitates will not form during the initial cooling of the weld bead, but will form during reheating above 500 °C in the ferrite temperature range [35]. In order to validate this prediction, samples were taken from the top bead of the 0.5V alloy, which did not undergo any reheating by subsequently deposited beads. The soaking treatment should not affect the precipitation state because of its low temperature. Several atom probe measurements of these top bead samples confirmed the prediction from the simulations: No signs of clustering or precipitation of V were found, allowing the conclusion that if precipitates form, they will form during reheating.

Secondly, the irregularity of the thermal history inside the all-weld metal has to be considered. The temperature profile in [35] can only serve as an example regarding both the number of peaks and the peak temperatures. Due to the occurring temperature fluctuations and gradients during welding of every bead, any arbitrarily chosen location in the weld metal will have a unique thermal history with a different number of reheating peaks and different peak temperatures ranging from 200 °C up to the melting point. Atom probe tomography is a locally very restricted method. The measured sample volume is very small (usually less than 1/1000 μm^3). Because it is impossible to predict the exact thermal history of a specific point in the all-weld metal, it was decided to capture the overall precipitation behavior of an alloy by taking 10 samples from random locations and averaging the gained results. As expected, the precipitate population was different for every sample of the same alloy. This also explains the occasionally high standard deviation in the average chemical composition of the precipitates.

However, the thermal history is not the only influence causing irregularities in the precipitation population. During solidification of the weld, interdendritic segregation of several alloying elements (especially Mn, Cr, Mo, but also V) occurs, leading to locally changing chemical compositions. Microprobe maps in Fig. 5 show elemental distributions of Mn, which segregates the most, and V. These segregations change the premises for precipitation of microalloy carbides or nitrides.

Despite these difficulties, a general trend of the precipitation behavior of differently microalloyed samples could be observed by averaging several measurements of every alloy. A combined addition of Ti, Nb, and Al resulted in the formation of Ti-rich carbonitrides (Table 4). Although Nb and Al can both induce precipitation in some steels [10], they played minor roles in this case (see also [35]).

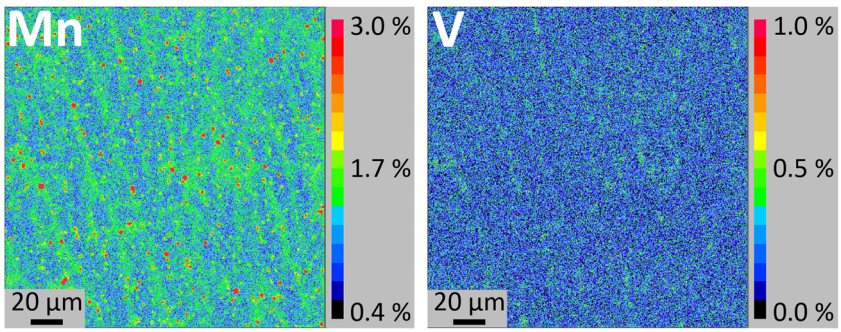

Fig. 5 Microprobe mapping of Mn and V in the all-weld metal showing interdendritic segregation. The red dots in the Mn mapping are Mn-rich inclusions, which do not affect the precipitate formation

The tendency of precipitate formation was strongly enhanced by additionally alloying V to this Ti-Nb-Al sample, causing bigger precipitates to form (Table 4). Much V was incorporated in the precipitates. This fact initiated the production of alloys containing only V as a microalloying element.

Very small clusters were observed in the 0.3V alloy, with V clustering first before attracting C and N to form very small precipitates. As the N content was very low in the samples alloyed only with V, it is no surprise that the precipitates in the 0.5V alloy, which were bigger in size, contained mainly C rather than N (Table 6).

At this point, it has to be mentioned, that with an addition of up to 0.5 m.% V, the term "microalloying" may not be feasible anymore. Nevertheless, this large amount of typical microalloying elements is necessary to increase the potential for clustering and precipitate formation, because the reheating peaks are very short. To some extent, it is surprising that precipitates up to 10 nm are formed during this short time after all.

The mechanical properties changed drastically with the addition of microalloying elements. Due to the precipitate formation, a strength increase of 100 MPa and more was achieved. However, an increase in V content from 0.2 or 0.3 to 0.5 m.% brought only little additional strength in both alloy groups, although the found precipitates were larger in both cases. Therefore, the first formation of many small clusters due to a moderate addition of V has much more effect on the strength than their growth.

Of course, with this strength increase, the remaining toughness of the alloy becomes an issue. Also, microalloying reduced the toughness of the investigated all-weld metals. However, with some adjustments in the alloy system, the toughness decrease can be kept to a minimum.

Overall, the concept of using the multi-layer design of the all-weld metal for precipitation of microalloy carbides and nitrides was successfully applied. The short reheating peaks were sufficient for precipitates to form, strengthening the all-weld metal significantly.

This proposed filler metal is intended for constructions in the as-welded condition. A post-weld heat treatment is assumed to be not applicable because of the high V content which might lead to severe precipitate growth and therefore deterioration of the toughness.

5 Conclusions

The effect of microalloying on ultra-high strength weld metal produced by gas metal arc welding was investigated regarding the existence of precipitates and their influence on the mechanical properties. The following conclusions can be drawn:

- Microalloying of all-weld metal with Ti, Nb, V, and Al yielded a significant strength increase.
- With atom probe tomography, it was shown that the strength increase resulted from nanometer-sized precipitates. Severe fluctuations in number density, size, and chemical composition of the precipitates were observed within every alloy.
- Ti and V showed a strong tendency for clustering. Nb was limitedly incorporated in the TiV precipitates. Al showed no signs of clustering in the all-weld metal.
- The precipitates did not form during the initial cooling of the weld, but during reheating by subsequently deposited weld beads.
- Due to inherent fluctuations in local thermal history and local chemical composition in the all-weld metal, an average precipitation state has to be evaluated from several measurements.

Acknowledgements Open access funding provided by Montanuniversity Leoben. The K-Project Network of Excellence for Metal JOINing is fostered in the frame of COMET - Competence Centers for Excellent Technologies by BMWFW, BMVIT, FFG, Land Oberösterreich, Land Steiermark, Land Tirol, and SFG. The program COMET is handled by FFG.

References

1. Evans GM (1995) Microstructure and properties of ferritic steel welds containing Al and Ti. Weld J 74:249s–261s
2. Vanovsek W, Bernhard C, Fiedler M, Schnitzer R (2013) Effect of titanium on the solidification and postsolidification microstructure of high-strength steel welds. Weld World 57:665–674. https://doi.org/10.1007/s40194-013-0063-1
3. Farrar RA, Harrison PL (1987) Acicular ferrite in carbon-manganese weld metals: an overview. J Mater Sci 22:3812–3820. https://doi.org/10.1007/BF01133327
4. Sugden A, Bhadeshia H (1989) Lower acicular ferrite. Metall Trans A 20:1811–1818
5. Babu SS, Bhadeshia HKDH (1991) Mechanism for the transition from bainite to acicular ferrite. Mater Trans 32:679–688
6. Keehan E, Karlsson L, Thuvander M, Bergquist E (2007) Microstructural characterisation of as-deposited and reheated weld metal—high strength steel weld metals. Weld World 51:44–49
7. Keehan E, Zachrisson J, Karlsson L (2010) Influence of cooling rate on microstructure and properties of high strength steel weld metal. Sci Technol Weld Join 15:233–238. https://doi.org/10.1179/136217110X12665048207692
8. Schnitzer R, Zügner D, Haslberger P, Ernst W, Kozeschnik E (2017) Influence of alloying elements on the mechanical properties of high-strength weld metal. Sci Technol Weld Join 22:536–543. https://doi.org/10.1080/13621718.2016.1274095

9. Haslberger P, Ernst W, Schnitzer R (2017) High resolution imaging of martensitic all-weld metal. Sci Technol Weld Join 22:336–342. https://doi.org/10.1080/13621718.2016.1240980
10. Gladman T (1997) The physical metallurgy of microalloyed steels. The Institute of Materials, London
11. Lagneborg R, Siwecki T, Zajac S, Hutchinson B (1999) The role of vanadium in microalloyed steels. Scand. J, Metall
12. Baker TN (2009) Processes, microstructure and properties of vanadium microalloyed steels. Mater Sci Technol 25:1083–1107. https://doi.org/10.1179/174328409X453253
13. Miller MK, Forbes RG (2009) Atom probe tomography. Mater Charact 60:461–469. https://doi.org/10.1016/j.matchar.2009.02.007
14. Marquis EA, Hyde JM (2010) Applications of atom-probe tomography to the characterisation of solute behaviours. Mater Sci Eng R Reports 69:37–62. https://doi.org/10.1016/j.mser.2010.05.001
15. Craven AJ, MacKenzie M, Cerezo A, Godfrey T, Clifton PH (2008) Spectrum imaging and three-dimensional atom probe studies of fine particles in a vanadium micro-alloyed steel. Mater Sci Technol 24:641–650. https://doi.org/10.1179/174328408X270347
16. Xie KY, Zheng T, Cairney JM et al (2012) Strengthening from Nb-rich clusters in a Nb-microalloyed steel. Scr Mater 66:710–713. https://doi.org/10.1016/j.scriptamat.2012.01.029
17. Enloe CM, Findley KO, Parish CM, Miller MK, de Cooman BC, Speer JG (2013) Compositional evolution of microalloy carbonitrides in a Mo-bearing microalloyed steel. Scr Mater 68:55–58. https://doi.org/10.1016/j.scriptamat.2012.09.027
18. Nöhrer M, Zamberger S, Primig S, Leitner H (2013) Atom probe study of vanadium interphase precipitates and randomly distributed vanadium precipitates in ferrite. Micron 54–55:57–64. https://doi.org/10.1016/j.micron.2013.08.008
19. Kapoor M, O'Malley R, Thompson GB (2016) Atom probe tomography study of multi-microalloyed carbide and carbo-nitride precipitates and the precipitation sequence in Nb-Ti HSLA steels. Metall Mater Trans A Phys Metall Mater Sci 47:1984–1995. https://doi.org/10.1007/s11661-016-3398-6
20. Isheim D, Kolli RP, Fine ME, Seidman DN (2006) An atom-probe tomographic study of the temporal evolution of the nanostructure of Fe-Cu based high-strength low-carbon steels. Scr Mater 55:35–40. https://doi.org/10.1016/j.scriptamat.2006.02.040
21. Wang H, Yu X, Isheim D, Seidman D, Babu SS (2013) High strength weld metal design through nanoscale copper precipitation. Mater Des 50:962–967. https://doi.org/10.1016/j.matdes.2013.03.093
22. Chen Y-S, Haley D, Gerstl SSA et al (2017) Direct observation of individual hydrogen atoms at trapping sites in a ferritic steel. Science (80-) 355:1196–1199. https://doi.org/10.1126/science.aal2418
23. Vitek JM, Babu SS (2011) Multiscale characterisation of weldments. Sci Technol Weld Join 16:3–11. https://doi.org/10.1179/1362171810Y.0000000003
24. Miller MK, Pareige P, Burke MG (2000) Understanding pressure vessel steels: an atom probe perspective. Mater Charact 44:235–254. https://doi.org/10.1016/S1044-5803(99)00056-X
25. Miller MK, Russell KF (2007) Embrittlement of RPV steels: an atom probe tomography perspective. J Nucl Mater 371:145–160. https://doi.org/10.1016/j.jnucmat.2007.05.003
26. Wang HH, Tong Z, Hou TP, Wu KM, Mehmood T (2017) Effects of evolution of nanoscale copper precipitation and copper content on mechanical properties of high-strength steel weld metal. Sci Technol Weld Join 22:191–197. https://doi.org/10.1080/13621718.2016.1213583
27. Edmondson PD, Miller MK, Powers KA, Nanstad RK (2016) Atom probe tomography characterization of neutron irradiated surveillance samples from the R. E. Ginna reactor pressure vessel. J Nucl Mater 470:147–154. https://doi.org/10.1016/j.jnucmat.2015.12.038
28. Kolli RP, Herzing AA, Ankem S (2016) Characterization of yttrium-rich precipitates in a titanium alloy weld. Mater Charact 122:30–35. https://doi.org/10.1016/j.matchar.2016.10.014
29. Mazumder B, Yu X, Edmondson PD et al (2016) Effect of friction stir welding and post-weld heat treatment on a nanostructured ferritic alloy. J Nucl Mater 469:200–208. https://doi.org/10.1016/j.jnucmat.2015.11.061
30. Choi KJ, Kim T, Yoo SC, Kim S, Lee JH, Kim JH (2016) Fusion boundary precipitation in thermally aged dissimilar metal welds studied by atom probe tomography and nanoindentation. J Nucl Mater 471:8–16. https://doi.org/10.1016/j.jnucmat.2015.12.047
31. Miller MK, Cerezo A, Hetherington MG, Smith GDW (1996) Atom probe field ion microscopy. Clarendon Press, Oxford
32. Miller MK, Forbes RG (2014) Atom-probe tomography: the local electrode atom probe. https://doi.org/10.1007/978-1-4899-7430-3
33. Larson DJ, Prosa TJ, Ulfig RM et al (2013) Local electrode atom probe tomography—a user's guide. Springer Science+Business Media, New York
34. Chen Y, Chou PH, Marquis EA (2014) Quantitative atom probe tomography characterization of microstructures in a proton irradiated 304 stainless steel. J Nucl Mater 451:130–136. https://doi.org/10.1016/j.jnucmat.2014.03.034
35. Schnitzer R, Zügner D, Haslberger P, et al (2016) IIW Document II-C-491-16: Influence of alloying elements on the mechanical properties of ultra-high strength weld metal